DOI: 10.1002/ejic.200800978

Valence-Tautomeric RbMnFe Prussian Blue Analogues: Composition and Time Stability Investigation

Lionel Salmon,[a] Esther J. M. Vertelman,[b] Carlos Bartual Murgui,[a] Saioa Cobo,[a] Gábor Molnár,[a] Petra J. van Koningsbruggen,*[b] and Azzedine Bousseksou*[a]

Keywords: Rubidium / Charge transfer / Nonstoichiometric compounds / Manganese / Iron

Three different stoichiometric forms of $Rb_xMn[Fe(CN)_6]_y \cdot zH_2O$ [$x = 0.96$, $y = 0.98$, $z = 0.75$ (**1**); $x = 0.94$, $y = 0.88$, $z = 2.17$ (**2**); $x = 0.61$, $y = 0.86$, $z = 2.71$ (**3**)] Prussian blue analogues were synthesized and investigated by magnetic, calorimetric, Raman spectroscopic, X-ray diffraction, and ^{57}Fe Mössbauer spectroscopic methods. Compounds **1** and **2** show a hysteresis loop between the high-temperature (HT) $Fe^{III}(S = 1/2)$–CN–$Mn^{II}(S = 5/2)$ and the low-temperature (LT) $Fe^{II}(S = 0)$–CN–$Mn^{III}(S = 2)$ forms of 61 and 135 K width centered at 273 and 215 K, respectively, whereas the third compound remains in the HT phase down to 5 K. The splitting of the quadrupolar doublets in the ^{57}Fe Mössbauer spectra reveal the electron-transfer-active centers. Refinement of the X-ray powder diffraction profiles shows that electron-transfer-active materials have the majority of the Rb ions on only one of the two possible interstitial sites, whereas nonelectron-transfer-active materials have the Rb ions equally distributed. Moreover, the stability of the compounds with time and following heat treatment is also discussed.

Introduction

Prussian blue analogues of transition metals with the general formula $A_xM[M'(CN)_6]_y \cdot zH_2O$ (where A is an alkali-metal cation, and M and M′ are generally first-row transition-metal cations) have attracted considerable interest because of their remarkable magnetic properties.[1–6] Within this family, several compounds present a first-order thermal phase transition associated with a metal-to-metal electron transfer.[7,8] Notably, the compound $Rb_xMn[Fe(CN)_6]_y \cdot zH_2O$ exhibits a charge-transfer (CT) phase transition between the high-temperature (HT) $Fe^{III}(S = 1/2)$–CN–$Mn^{II}(S = 5/2)$ and the low-temperature (LT) $Fe^{II}(S = 0)$–CN–$Mn^{III}(S = 2)$ states, either of which displays markedly different magnetic, optical, and electronic properties.[8–25] The transition between the two phases can be induced not only by changing the sample temperature, but also by applying external pressure or by light irradiation.[12]

In compounds having the idealized formula $RbMn[Fe(CN)_6]$, the ground state at low temperatures is the Fe^{II}_{LS}–CN–Mn^{III}_{HS} (LS = low spin, HS = high spin) configuration. However, at high temperatures, the Fe^{III}_{LS}–CN–Mn^{II}_{HS} configuration becomes the thermodynamically stable phase as a result of its higher entropy of electronic and vibrational origins. In contrast, the phase-transition temperature depends strongly on the actual sample stoichiometry.[14] In fact, in compounds with vacant $Fe(CN)_6$ sites, oxygen atoms of water molecules coordinate to the Mn ions instead of the nitrogen atoms of the cyanide ions and the average environment of the manganese ions changes to $Mn(OH_2)_x(NC)_{6-x}$. The formation of these vacancies leads to a lower Rb^+ proportion in order to maintain the charge neutrality. As a result, the ligand field strength of the Mn ions becomes weaker, and consequently, the redox potential of the Mn^{III}/Mn^{II} couple decreases, which leads finally to its inability to reduce $[Fe^{III}(CN)_6]$ to $[Fe^{II}(CN)_6]$. If the water content is sufficiently high, the redox potential decreases to such an extent that the Fe^{III}_{LS}–CN–Mn^{II}_{HS} form becomes stable at very-low temperatures.[21] This important role of the incorporated water molecules, which may be coordinated as well as noncoordinated, suggests that the physical properties of these compounds may change with time, but to the best of our knowledge, this occurrence has not been discussed in the literature. It is also important to note that the transition from the HT to LT form is accompanied by a remarkable volume contraction of ca. 10% associated with a structural change from cubic (*F-43m*) to tetragonal (*I-4m2*) owing to the Jahn–Teller distortion of the Mn^{III} ion in the LT phase.[9]

In this paper, we report on the syntheses and detailed physical characterization of three novel compounds of $Rb_xMn[Fe(CN)_6]_y \cdot zH_2O$ with different stoichiometries: $Rb_{0.96}Mn[Fe(CN)_6]_{0.98} \cdot 0.75H_2O$ (**1**), $Rb_{0.94}Mn[Fe(CN)_6]_{0.88} \cdot$

[a] Laboratoire de Chimie de Coordination, CNRS UPR-8241, 205 Route de Narbonne, 31077 Toulouse, France
E-mail: boussek@lcc-toulouse.fr
[b] Stratingh Institute for Chemistry, University of Groningen, Nijenborgh 4, 9747 AG Groningen, The Netherlands
E-mail: P.J.van.Koningsbruggen@rug.nl

Supporting information for this article is available on the WWW under http://www.eurjic.org or from the author.

$2.17H_2O$ (**2**), and $Rb_{0.61}Mn[Fe(CN)_6]_{0.86}\cdot 2.71H_2O$ (**3**), and we discuss the effect of the stoichiometry change on their crystallographic and electronic structure, as well as on their spectroscopic and magnetic properties.

Results and Discussion

Sample 1

The $\chi_M T$ value, where χ_M stands for the molar magnetic susceptibility and T for temperature, of freshly prepared compound **1** decreases abruptly from 4.6 to 3.2 $cm^3\,K\,mol^{-1}$ around 250 K upon cooling, and conversely, as the sample is warmed up from 130 K, the $\chi_M T$ value increases around 300 K and reaches the initial $\chi_M T$ value (Figure 1). The values of $\chi_M T$ in the high-and low-temperature regions are in agreement with the theoretical values expected for the sum of the spin only values of $Fe^{III}{}_{LS}$-$Mn^{II}{}_{HS}$ and $Fe^{II}{}_{LS}$-$Mn^{III}{}_{HS}$, respectively, thus revealing a complete transition, which would indeed be in agreement with an approximately 1:1 Mn/Fe ratio. The width of the thermal hysteresis loop (61 K) is defined by $T_{1/2}\downarrow$ = 242 K and $T_{1/2}\uparrow$ = 303 K. These temperatures correlate with the general trends reported in ref. [14], that is, when the Rb content is close to 1 and the water content tends to go towards zero, the phase transition shifts to higher temperatures and the hysteresis width decreases (see Supporting Information). The magnetic measurements on this sample were reproduced after the compound had aged for six months under ambient storage conditions. These reveal a smaller hysteresis ($T_{1/2}\downarrow$ = 250 K and $T_{1/2}\uparrow$ = 303 K) and an upward displacement of the absolute values of $\chi_M T$ (Figure 1). On the whole, however, if one takes into account the measurement uncertainties the overall difference appears to be relatively small.

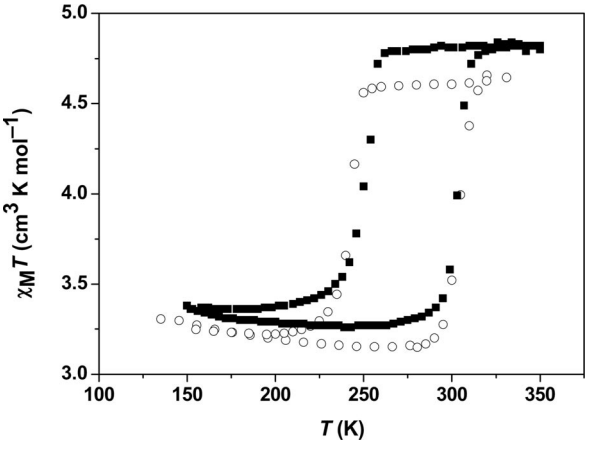

Figure 1. Temperature dependence of $\chi_M T$ of **1** in the cooling and heating modes: (○) freshly prepared sample, (■) after 6 months storage under ambient conditions.

The first-order phase transition in an aged sample of **1** was also evidenced by differential scanning calorimetric (DSC) measurements (Figure 2) and the associated enthalpy and entropy changes were determined as ΔH = 15 $kJ\,mol^{-1}$ and ΔS = 53 $J\,K^{-1}\,mol^{-1}$. These values are in agreement with the literature data.[14,24] As discussed in ref.[14] this large entropy change has, for the most part, a vibrational origin. The completeness of the transition was confirmed by Raman spectroscopy (Figure 3), which revealed two CN stretching modes in the HT phase around 2159 and 2168 cm^{-1} (indicative of CN stretching in Fe^{III}–CN–Mn^{II}), whereas the LT phase is characterized by two modes around 2094 and 2113 cm^{-1} (CN stretching in Fe^{II}–CN–Mn^{III}). The sharp peaks observed in the Raman spectra [FWHM (full-width half-maximum) = ca. 3.5 cm^{-1}] confirm nicely the proposed correlation between the stoichiometry of the samples and the Raman linewidths, that is, the more deviation from a "perfect" stoichiometry, the broader the lines in the CN stretching region (see Supporting Information).[14]

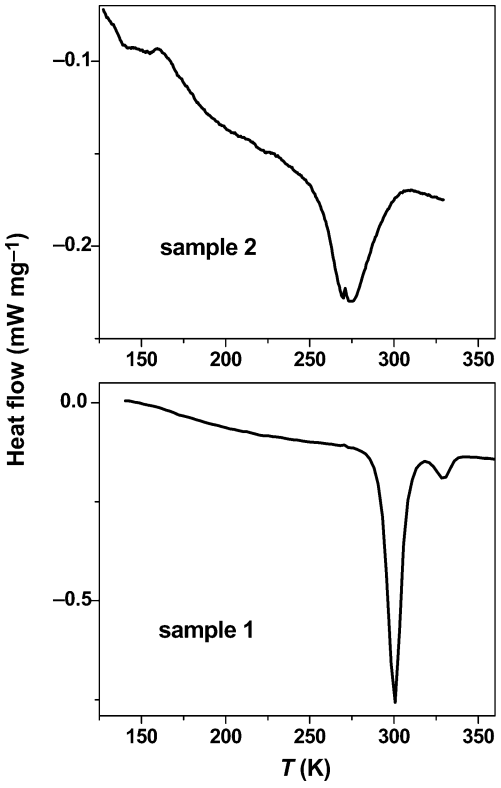

Figure 2. DSC curves recorded in the heating mode for samples **1** and **2**.

Selected ^{57}Fe Mössbauer spectra of aged compound **1** acquired in the cooling and heating modes (HT and LT phases, respectively) within the hysteresis region at 265 K are shown in Figure 4. Values of the hyperfine parameters obtained from the least-squares fitting procedure of the spectra recorded in the 293–80 K region are listed in Table 1. In the cooling mode at 265 K the spectrum corresponding to $Fe^{III}{}_{LS}$ (HT phase) can be fitted with a doublet with an isomer shift δ = –0.133(2) $mm\,s^{-1}$ and a quadrupole spitting QS = 0.097(2) $mm\,s^{-1}$. In the heating process, the spectrum corresponding to $Fe^{II}{}_{LS}$ (LT phase) can be fitted with a doublet with an isomer shift δ = –0.119(1) $mm\,s^{-1}$ and a quadrupole spitting QS = 0.124(8) $mm\,s^{-1}$. In other

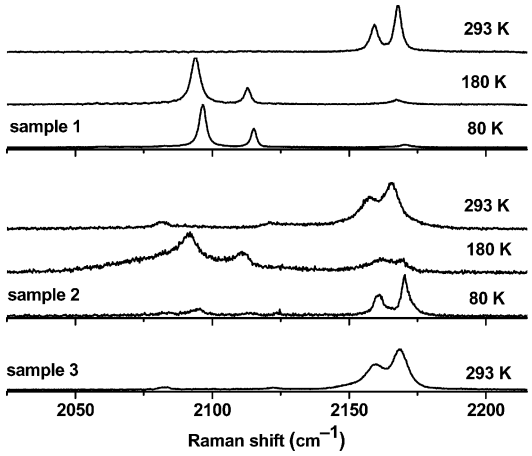

Figure 3. Raman spectra of samples **1**, **2**, and **3** acquired at 293 (cooling mode), 80 (cooling mode), and 180 K (heating mode).

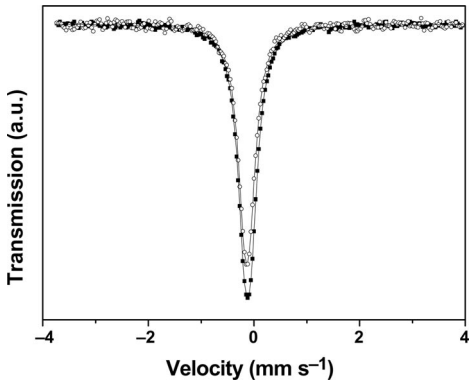

Figure 4. ^{57}Fe Mössbauer spectra of **1** acquired at 265 K in the cooling (○) and heating (■) modes with fitted line.

words, taking into account the Mössbauer hyperfine parameters, distinguishing the two forms is not straightforward. However, the Mössbauer peak areas appear significantly different, indicating that the recoilless fractions differ in the two phases. Indeed, the plot of the total area (A) as a function of the temperature (Figure 5) reveals clearly a discontinuity at the phase transition. This sudden change in A reflects a marked variation in the Lamb–Mössbauer factor, that is, in the lattice dynamics. In a more quantitative manner, by using the Debye model in the high temperature limit one can determine the so-called "Mössbauer Debye temperature", θ_D from the temperature dependence of A by using the relationship:[26,27]

$$d(\ln[A])/dT = -3E_\gamma^2/Mc^2k_B\theta_D^2$$

where E_γ is the Mössbauer transition energy, k_B is the Boltzmann constant, c is the velocity of light, and M has been taken as the mass of the "bare" Mössbauer atom (^{57}Fe in the present case). A linear least-squares fit of ln[A] vs. T allowed us to determine the values of θ_D as 265(±24) K and 333(±14) K in the HT and LT phases, respectively. The higher value of θ_D in the LT phase signifies that the crystal lattice is more rigid in this phase. This finding is in nice agreement with the X-ray diffraction data,[9] which reveals a strong lattice contraction when going from the HT to the LT phase and also with the calorimetric results, which indicate a significantly higher vibrational entropy in the HT phase.

The X-ray powder diffraction profile of sample **1** obtained at room temperature (see Supporting Information)

Table 1. Least-squares fitted Mössbauer data for sample **1** obtained in the cooling (293–80 K) and heating (265 and 293 K) modes. Values in parentheses are the error bars of statistical origin. Italicized values were fixed during the fitting.

	Doublet				Doublet		
T (K)	IS[a] (mm s^{-1})	QS[b] (mm s^{-1})	$\Gamma/2$[c] (mm s^{-1})	Area (%)	IS[a] (mm s^{-1})	QS[b] (mm s^{-1})	$\Gamma/2$[c] (mm s^{-1})
293	–0.151(2)	0.07(2)	0.152(5)	100			
285	–0.138(3)	0.177(9)	0.162(7)	100			
275	–0.137(2)	0.159(7)	0.155(5)	100			
265	–0.133(2)	0.097(2)	0.162(7)	100			
255	–0.131(1)	0.049(3)	0.155(5)	100			
245	–0.126(2)	0.026(8)	0.157(8)	100			
235	–0.123(3)	*0*	0.17(1)	100			
225	*–0.121*	*0.12*	*0.16*	78(6)	*–0.094*	*0.12*	*0.16*
215	*–0.117*	*0.12*	*0.16*	53(9)	*–0.091*	*0.12*	*0.16*
205	*–0.114*	*0.12*	*0.16*	20(10)	*–0.087*	*0.12*	*0.16*
195					–0.086(2)	0.117(9)	0.16(4)
180					–0.080(2)	0.12(1)	0.168(6)
160					–0.074(4)	0.145(2)	0.159(9)
140					–0.069(2)	0.12(1)	0.164(7)
120					–0.060(2)	0.13(1)	0.159(7)
100					–0.054(1)	0.117(7)	0.156(3)
80					–0.050(2)	0.12(1)	0.151(6)
265					–0.119(1)	0.124(8)	0.165(4)
293					–0.147(1)	0.11(1)	0.164(4)

[a] IS: isomer shift (with reference to metallic iron at 293 K). [b] QS: quadrupole splitting. [c] Γ: half-height width.

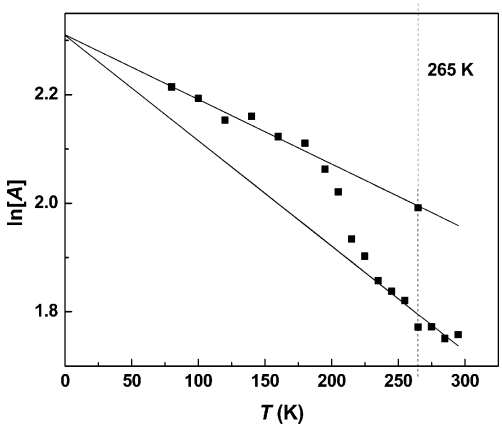

Figure 5. Temperature dependence of the natural logarithm of the total area of ^{57}Fe Mössbauer spectra of **1**. The lines represent linear fits on data obtained in the pure LT and HT phases.

was satisfactorily fitted by using the *F-43m* model previously reported by Vertelman et al.[22] The atom fractions on each crystallographic site were fixed to those obtained from the elemental analysis, with the exception of the fractions of the Rb and O atoms. For Rb, there are two crystallographic distinct positions in the *F-43m* phase: *4c* and *4d* (hereafter denoted as Rb1 and Rb2, respectively). We assume that the octahedral environment of the Mn ion is always maintained by coordination of water molecules; therefore, the O3 fraction was kept constant on 0.02. During structural refinement, a series of constraints involving the Rb and O fractions were set up: [Rb1] + [Rb2] = 0.96, [O1] + [O2] = 0.63 (= 0.75–6 × 0.02), [Rb1] + [O1] = 0.96, and [Rb2] + [O2] = 0.63. Unfortunately, (small) negative fractions occurred for Rb2 and O1. Because this does not make sense chemically, all Rb ions were placed on Rb1 and the remaining O atoms were placed on O2. Constraints were also placed on the isotropic atomic displacement parameters, *U*iso: $U\text{iso}_{\text{Mn}} = U\text{iso}_{\text{Fe}}$, $U\text{iso}_{\text{Rb1}} = U\text{iso}_{\text{Rb2}} = U\text{iso}_{\text{O1}} = U\text{iso}_{\text{O2}}$, $U\text{iso}_{\text{C}} = U\text{iso}_{\text{N}} = U\text{iso}_{\text{O3}}$. The determined Fe–C and Mn–N distances of 1.86(4) and 2.28(3) Å are indicative of LS Fe^{III} and HS Mn^{II}, respectively, and match those in the previously reported single-crystal structure of the HT configuration [Fe–C 1.929(4) Å, Mn–N 2.205(5) Å], by taking into account the uncertainties in the present model.[22] After refinement of the profile by using this cubic model, weak unindexed peaks were still present at 2θ values of 24.5 and 35°. These peaks are indicative of the LT phase (space group *I-4m2*) reported by Moritomo et al.[10]

Sample 2

Figure 6a shows the product of the molar magnetic susceptibility and the temperature for freshly prepared sample **2** as a function of temperature measured at a rate of 2 and 0.3 K min^{-1}, respectively. At room temperature the $\chi_M T$ value is ca. 4.6 cm^3 K mol^{-1}. The first cooling was carried out at a rate of 2 K min^{-1} and a partial transition was observed between 160 and 130 K leading to a partially quenched HT phase. At 80 K, the $\chi_M T$ value reaches ca. 4.0 cm^3 K mol^{-1}, which corresponds to a mixture of ca. 40% LT and 60% HT phase. In the heating mode, around 130 K, the quenched, metastable HT phase relaxes and consequently the $\chi_M T$ value decreases to ca. 3.5 cm^3 K mol^{-1}. This value indicates the presence of a residual HT fraction even after the relaxation. As shown in Figure 6a, if the sample is slowly cooled down at a rate of 0.3 K min^{-1} one can avoid quenching the system. The width of the thermal hysteresis loop (135 K) is defined by $T_{1/2}\downarrow$ = 147 K and $T_{1/2}\uparrow$ = 282 K. Such a large hysteresis width is an appealing property for the application of these materials in various devices (e.g., memories). It is interesting to note that in the warming mode for both experiments, the phase transition occurs in two steps with a very small plateau around 280 K. This unprecedented result may have a crystallographic origin. The two steps are also reflected in the DSC curve of the sample (Figure 2).

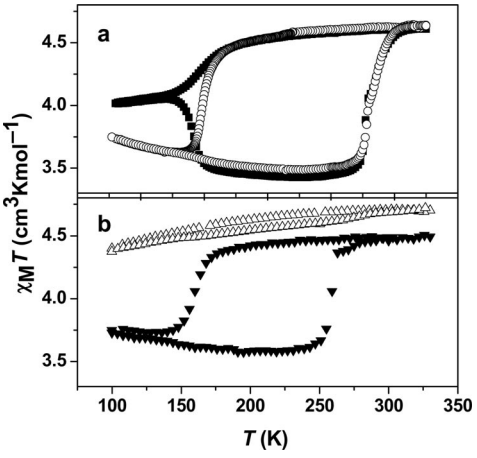

Figure 6. (a) Temperature dependence of $\chi_M T$ of freshly prepared sample **2** recorded at different cooling rates: 2 (■) and 0.3 K min^{-1} (○). (b) Temperature dependence of $\chi_M T$ (recorded at 0.3 K min^{-1} cooling rate) of **2** after 1 month ageing (Δ), followed by a heat treatment at 403 K (▼).

The incomplete nature of the transition in sample **2** was confirmed by Raman spectroscopy (Figure 3), which revealed the presence of a small fraction of the reduced Fe^{II}_{LS}–CN–Mn^{II}_{HS} form (υ_{CN} = 2082 and 2120 cm^{-1}) in the HT phase and a significant quantity of residual Fe^{III}_{LS}–CN–Mn^{II}_{HS} form (υ_{CN} = 2161 and 2169 cm^{-1}) in the LT phase at 180 K (heating mode). It should be noted that at 80 K the Raman spectrum of this compound corresponds to the HT phase even if the sample is cooled down at a very slow cooling rate. This observation reflects the fact that the exciting laser light instantaneously transforms the LT phase into the HT phase, which then remains trapped due to the slow relaxation kinetics at this temperature.

The stoichiometry of sample **2** deviates significantly from the general trend observed previously[14] (see Supporting Information), which means that the sample does not consist of a homogeneous phase. This fact is also reflected in the Raman and Mössbauer spectra. It is therefore difficult to

discuss in this case the correlation between the sample stoichiometry and the phase-transition temperatures. In contrast, it is possible to measure the broadening of the Raman spectral lines, which correspond to the HT phase. It appears that the two CN stretching modes in the HT phase display a significant line broadening: the FWHM values measured at room temperature are 4.9 and 6.0 cm^{-1} for the modes centered around 2170 and 2159 cm^{-1}, respectively. This line broadening is in fairly good agreement with the relatively large amount of $Fe(CN)_6^{3-}$ vacancies and also with the observed phase-transition temperatures (see Supporting Information).

Sample **2** appeared to be unstable under ambient storage conditions. As shown in Figure 6b, only a small fraction (ca. 5%) of the compound exhibits a charge transfer after one month. This temporal evolution of sample **2** towards the HT phase suggests that an additional amount of water molecules entered the crystal lattice to such an extent that the Fe^{III}_{LS}–CN–Mn^{II}_{HS} form becomes stable whatever the temperature. The most plausible explanation of this phenomenon is water uptake from the air. Indeed, one should notice that this sample contains a large amount of $Fe(CN)_6^{3-}$ vacancies and the coordination sphere of manganese ions must be completed somehow. If this hypothesis is correct, a supplementary heat treatment may allow removal of a certain amount of water molecules and the charge transfer should thus be restored. We have thus carried out a thermal treatment on sample **2** (HT form) in an oven at 130 °C for 5 d. As shown by the magnetic measurements (Figure 6b), the sample exhibits a large hysteresis loop following this treatment even if the final phase-transition temperatures are somewhat different from those observed in the starting material.

Mössbauer spectra of compound **2** (freshly prepared) at selected temperatures are shown in Figure 7 and values of the hyperfine parameters obtained from the least-square fitting procedure are listed in Table 2 for each spectrum. At room temperature, the Mössbauer spectrum can be satisfactorily fitted by using three components: two quadrupolar doublets and one singlet with approximately 40:45:15 area-% ratios. On the basis of the hyperfine parameters and the strong temperature dependence of the quadrupole splitting, the doublets can be clearly assigned to low-spin (LS) iron(III) species in two different distorted cubic environments.[26] On the sole basis of the isomer shifts, the singlet component can be assigned either to LS iron(II) or LS iron(III) in a local cubic symmetry. Nevertheless, in agreement with the Raman results, the singlet component can be straightforwardly attributed to a LS iron(II) species corresponding to the reduced form of the complex (Fe^{II}–Mn^{II}). The temperature dependence of the Mössbauer parameters indicates that the species with the largest quadrupole splitting (about 45 area-% ratio) is not involved in the phase transition. When the sample is cooled down to 170 K, the area of the LS iron(III) doublet with the small quadrupole splitting decreases and, conversely, the area of the LS iron(II) singlet increases. At 80 K, this iron(III) species is converted almost completely into the corresponding iron(II) species. The main finding here is that the Mössbauer data gives unambiguous evidence for the existence of two structurally different LS iron(III) environments in the sample at room temperature, with only one of them being involved in the thermal phase transition. This result is similar to what we have found in single crystals of this compound and the difference between the two iron sites must

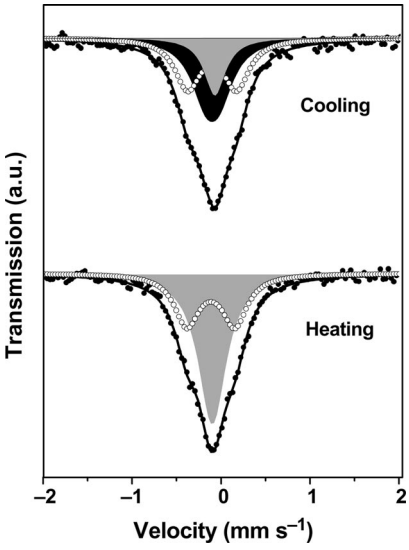

Figure 7. ^{57}Fe Mössbauer spectra (●) of **2** acquired in the cooling and heating modes at 210 K with fitted line consisting of three subspectra: two doublets (black shaded area and ○) [LS iron(III)] and one singlet (grey shaded area) [LS iron(II)].

Table 2. Least-squares fitted Mössbauer data for sample **2** obtained in the cooling (293–80 K) and heating (170 and 210 K) modes. Values in parentheses are the error bars of statistical origin. Italicized values were fixed during the fitting.

	Doublet				Doublet				Singlet		
T (K)	IS[a] ($mm\,s^{-1}$)	QS[b] ($mm\,s^{-1}$)	$\Gamma/2$[c] ($mm\,s^{-1}$)	Area (%)	IS[a] ($mm\,s^{-1}$)	QS[b] ($mm\,s^{-1}$)	$\Gamma/2$[c] ($mm\,s^{-1}$)	Area (%)	IS[a] ($mm\,s^{-1}$)	$\Gamma/2$[c] ($mm\,s^{-1}$)	Area (%)
293	–0.15(1)	0.46(1)	0.153(8)	45(8)	*–0.15*	*0.13*	0.14(2)	39(10)	–0.099(6)	0.118(6)	16(3)
210	–0.116(8)	0.55(1)	0.175(5)	44(2)	–0.12(1)	0.170(5)	0.20(1)	38(3)	–0.08(1)	0.150(5)	18(2)
170	–0.10(1)	0.64(1)	0.173(6)	42(6)	–0.090(2)	*0.23*	0.15(2)	42(4)	–0.067(3)	0.160(1)	16(3)
140	–0.08(1)	0.70(1)	0.166(5)	36(4)	–0.075(3)	*0.28*	0.15(2)	29(6)	–0.055(2)	0.160(9)	35(4)
80	–0.076(8)	0.77(2)	0.181(2)	36(1)	*–0.065*	*0.34*	0.12(6)	3(2)	–0.049(4)	*0.21*	61(2)
170	–0.103(7)	0.62(3)	0.172(3)	34(1)					–0.079(3)	0.20(2)	66(2)
210	–0.113(1)	0.54(1)	0.169(5)	37(2)					–0.097(5)	0.19(5)	63(3)

[a] IS: isomer shift (with reference to metallic iron at 293 K). [b] QS: quadrupole splitting. [c] Γ: half-height width.

Table 3. Least-squares fitted Mössbauer data for sample **2** following rapid cool down to 20 K. Values in parentheses are the error bars of statistical origin. Italicized values were fixed during the fitting.

	Doublet			Doublet			Singlet		Sextet		
T (K)	IS[a] (mm s^{-1})	QS[b] (mm s^{-1})	$\Gamma/2$[c] (mm s^{-1})	IS[a] (mm s^{-1})	QS[b] (mm s^{-1})	$\Gamma/2$[c] (mm s^{-1})	IS[a] (mm s^{-1})	$\Gamma/2$[c] (mm s^{-1})	IS[a] (mm s^{-1})	H (kOe)	Area (%)
20	–0.076(7)	0.847(6)	0.190(4)	–0.072(8)	0.346(5)	0.184(9)	–0.040(2)	*0.21*			42/38/20/0
15	–0.069(7)	0.86(2)	*0.21*	*–0.070*	*0.36*	*0.21*	*–0.021*	*0.21*	–0.14(1)	130.5(7)	34/11/14/41
10							–0.01(1)	*0.21*	–0.08(1)	184.8(9)	0/0/12/88
5							0.00(1)	*0.21*	–0.07(1)	191.4(8)	0/0/11/89

[a] IS: isomer shift (with reference to metallic iron at 293 K). [b] QS: quadrupole splitting. [c] Γ: half-height width.

probably be traced back to the different occupation of the interstitial sites either by rubidium ions or by water molecules.[22]

To investigate the electronic state of the quenched HT phase, compound **2** (freshly prepared) was cooled down to 5 K at a rate of 20 K min^{-1} and Mössbauer spectra were measured between 5 and 20 K (Figure 8, Table 3). At 20 K, the spectra can be satisfactorily fitted by using three components; two quadrupolar doublets and one singlet with approximately 42:38:20 area-% ratios. The similar proportions determined at room temperature confirm the total quench of the system. At 15 K, the intensities of both quadrupole doublets start to decrease and an enlarged magnetic component appears spontaneously. Below 15 K, the magnetic sextet was fitted by a least-squares fitting procedure, and the obtained local magnetic hyperfine field has a value of about 200 kOe. This value is much higher than predicted by the $-220<S_z>$ rule for a single unpaired electron, but presumably there will also be orbital and dipolar terms.[26] These findings are in reasonable agreement with the report of Ohkoshi et al.[20] who revealed an antiferromagnetic ordering around 11.5 K in the HT phase by neutron diffraction measurements.

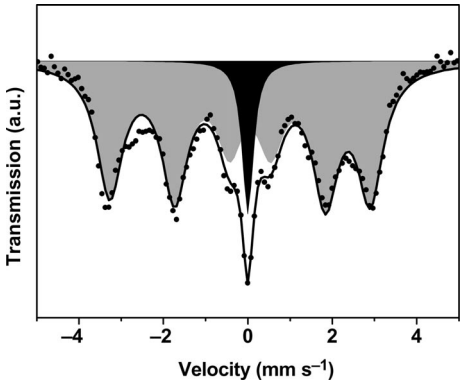

Figure 8. ^{57}Fe Mössbauer spectrum (●) of the quenched HT phase of **2** recorded at 5 K with fitted line consisting of two subspectra: one sextet (grey shaded area) [LS iron(III)] and one singlet (black shaded area) [LS iron(II)].

Sample 3

Figure 9 displays the evolution of the molar magnetic susceptibility of sample **3** as a function of temperature. The magnetic behavior clearly shows that the sample does not exhibit an electron transfer, which is in agreement with the literature for a $Rb_xMn[Fe(CN)_6]_y\cdot zH_2O$ compound with this stoichiometry.[14,21] The $\chi_M T$ value at room temperature is 4.75 cm^3 K mol^{-1}. This value is exactly what would be expected for a paramagnetic $\{S_1{:}S_2\} = \{5/2{:}1/2\}$ spin system. The room-temperature Raman spectrum of sample **3** is characterized by two large CN stretching modes around 2159 and 2168 cm^{-1} with FWHM = 9.2 and 6.0 cm^{-1}, respectively (Figure 3). These large linewidths are due to the significant deviation from a perfect $RbMn[Fe(CN)_6]$ stoichiometry of the sample and correlate nicely with the lack of charge transfer in this sample (see Supporting Information). The Raman spectrum reveals also the presence of a small amount of the reduced form in this sample (2122 and 2082 cm^{-1}) besides the HT form. This reduced form appears also from the fit of the room-temperature Mössbauer spectrum, which displays a singlet and a quadrupolar doublet (Figure 10, Table 4). Indeed, the former species can be assigned to a small amount of ferrous species, whereas the latter is attributed to ferric ions. It is interesting to note the relatively large quadrupole splitting (0.44 mm s^{-1}) in the iron(III) subspectrum. This value is comparable with values observed in sample **2**, as well as in single crystals of $RbMn[Fe(CN)_6]\cdot H_2O$ for the ferric ions that do not show electron transfer.[22] This is in contrast with the case of the electron-transfer-active iron(III) species (observed in samples **1** and **2** as well as in single crystals[22]), which display either a singlet or a doublet with very small quadrupole splitting (ca. 0.15 mm s^{-1}) in their ^{57}Fe Mössbauer spectrum at room temperature. One may suggest therefore that the more the environment of the Fe^{III} ion deviates from the perfect cubic symmetry of the Prussian blue structure, the more the quadrupole splitting increases. In this way, the room temperature Mössbauer spectrum is a direct measure of the electron-transfer efficiency to be detected at lower temperatures.

The X-ray diffraction profile of sample **3** was fitted in the same way as for sample **1** (see Supporting Information). For Rb and O two scenarios were tested: one in which the Rb ions were equally distributed over the two interstitial sites (*4c* and *4d*) and the vacancies on these sites were filled by O atoms, and one in which all the Rb ions were placed on the *4c* position and the remaining vacancies on both sites were filled by O atoms. Of these two scenarios the first

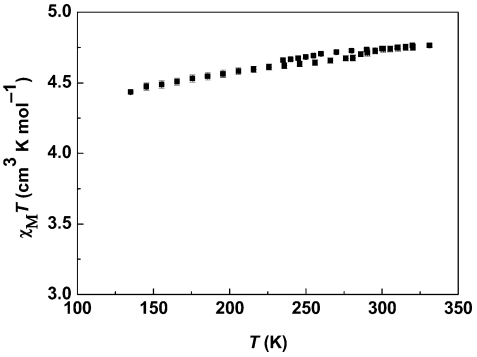

Figure 9. Temperature dependence of $\chi_M T$ of **3** in the cooling and heating modes.

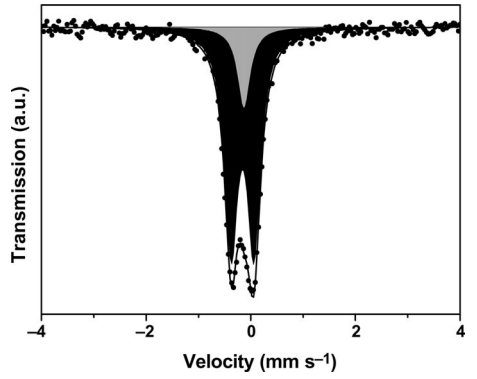

Figure 10. ^{57}Fe Mössbauer spectrum (●) of **3** acquired at 295 K with fitted line consisting of two subspectra: one doublet (black shaded area) [LS iron(III)] and one singlet (grey shaded area) [LS iron(II)].

Table 4. Least-squares fitted Mössbauer data for sample **3**. Values in parentheses are the error bars of statistical origin.

Doublet (293 K)	
IS[a] (mm s^{-1})	–0.156(4)
QS[b] (mm s^{-1})	0.44(2)
$\Gamma/2$[c] (mm s^{-1})	0.155(9)
Area (%)	84(13)
Singlet (293 K)	
IS[a] (mm s^{-1})	–0.13(1)
$\Gamma/2$[c] (mm s^{-1})	0.15(7)

[a] IS: isomer shift (with reference to metallic iron at 293 K). [b] QS: quadrupole splitting. [c] Γ: half-height width.

clearly gave the best agreement. Unfortunately, refinement of the fractions of Rb and O led to an unstable refinement. The determined Fe–C and Mn–N distances were 1.98(2) and 2.16(2) Å, respectively, which are close to the values found for single crystals.[22] The profile showed the same weak unindexed peaks as in the profile of sample **1**. From the refinement of our X-ray powder diffraction profiles combined with findings reported in the literature[10,11,22,25] it is clear that in the structure of compounds that are electron-transfer active, the majority of the Rb ions are located on the *4c* position in the *F-43m* space group and the noncoordinated water molecules are located on the *4d* position; this result is in good agreement with those reported by the group of Ohkoshi on similar compounds.[25] Therefore, it appears that besides a favorable stoichiometry, the distribution of the Rb ions and water molecules over the interstitial sites is also of crucial importance for determining the electron-transfer activity. Indeed, in the case of single crystals[22] we have shown that even a difference of 75:25 in the distribution of the Rb ions over the two interstitial sites leads to a reduction of 50% in the electron-transfer efficiency.

Conclusions

The physical and spectroscopic characterization of $Rb_xMn[Fe(CN)_6]_y{\cdot}zH_2O$ samples with different stoichiometries allowed us to observe in which way the spectral (Raman and Mössbauer) and structural characteristics as well as the charge-transfer (CT) phase transition vary with the sample stoichiometry. In samples with a stoichiometry that is close to Rb/Mn/Fe, 1:1:1, the transition is more complete and the hysteresis loop is relatively narrow. Furthermore, the linewidths of the modes present in the CN stretching region in Raman spectra become narrower. This is in line with our previous findings.[14] An unprecedented finding of this paper is that the temporal stabilities of the samples depend strongly on the synthetic conditions. In certain cases (samples **1** and **3**), the magnetic properties and notably the CT phase transition appears quite stable for several months, but in the case of sample **2** the phase transition is completely suppressed within a few weeks. Interestingly, heat treatment allows the recovery of the phase transition suggesting that exchange of water molecules between the lattice and the atmosphere has a huge influence on the magnetic properties. Further investigation of this phenomenon might be interesting in view of the application of this material in humidity sensors.

Another new feature in this manuscript is that the room-temperature ^{57}Fe Mössbauer spectra give a direct measure of the amount of electron-transfer-active material present in the sample. The part of the material that is electron-transfer active shows a doublet with a small quadrupole splitting (≈0.10 mm s^{-1}) for LS Fe^{III}, indicating a very small deviation from cubic symmetry. In contrast, the part that is not active shows a doublet with significant larger quadrupole splitting (>0.45 mm s^{-1}). The relative areas of these doublets are directly proportional to the fraction of electron-transfer-active material present in the sample. It is interesting to note, in contrast, that the hyperfine Mössbauer parameters do not allow for a straightforward distinction between the LS ferrous and ferric species in the LT and HT phases and the transition is better observed through the variation of the Lamb–Mössbauer factors.

From the refinement of the X-ray powder diffraction profiles it may be concluded that in electron-transfer-active materials the majority of the Rb^+ ions is located on one of the two possible interstitial sites, thereby presumably ensuring the cubic environment of the Fe and Mn ions. In con-

trast, in nonelectron-transfer-active materials the Rb ions appear to be equally distributed over the two interstitial sites, thus apparently contributing to creating a less cubic environment for the metal ions.

Experimental Section

Syntheses: All chemicals purchased from Sigma–Aldrich were of analytical grade and used without further purification.

1: A solution of $MnCl_2{\cdot}4H_2O$ (0.495 g, 2.5 mmol) in H_2O (25 mL, room temperature) was added to a solution of $K_3[Fe(CN)_6]$ (0.823 g, 2.5 mmol) and RbCl (3.023 g, 25 mmol) in H_2O (25 mL, 43 °C). The resulting solution was stirred. The addition speed was kept constant to 6 mL h^{-1} with a syringe pump model 352 of Sage Instruments. A brown powder precipitated and this was centrifuged and washed with room-temperature water (2×). The sample was dried overnight in vacuo. Yield (based on Mn): 653 mg (73%). $Rb_{0.96}Mn[Fe(CN)_6]_{0.98}{\cdot}0.75H_2O$ (358.10): calcd. C 19.76, H 0.42, Fe 15.32, Mn 15.33, N 23.05, Rb 22.79; found C 20.34, H <0.20, Fe 15.44, Mn 15.33, N 22.80, Rb 22.79.

2: In contrast to the "usual" synthesis route of compounds **1** and **3**, which were obtained from a pure aqueous solution, compound **2** was obtained from a water/ethanol mixture by instantaneous mixing a ethanolic solution (3 mL) of $MnCl_2{\cdot}4H_2O$ (0.1 M) and an aqueous solution (3 mL) containing both $K_3Fe(CN)_6$ (0.1 M) and RbCl (0.8 M). All solutions were heated to a temperature of 50 °C before the addition procedure. The brown powder precipitate was filtered, washed with water (2×), and dried in air at room temperature. Yield (based on Mn): 89 mg (82%). For sample **2**, it was not possible to determine an accurate chemical formula because of its instability and also because of the significant mixture of different valencies of iron in this compound. The elemental analysis gave Rb 22.42%, Mn 15.23%, and Fe 13.69%, from which we derived only the relative proportions of the metal ions as Rb/Mn/Fe, 0.94:1:0.88, and an approximate formula as $Rb_{0.94}Mn[Fe(CN)_6]_{0.88}{\cdot}2.17H_2O$ (360.79). The magnetic, Raman, Mössbauer, and DSC measurements, reported above, were performed on freshly prepared samples, but the acquisition of Mössbauer data took more than one week. It should be noted also that the thermodynamic parameters (ΔH, ΔS) as well as the molar magnetic susceptibility could not be accurately evaluated for this sample due to the approximated molar mass and also the relatively high amount of residual fractions remaining unaltered during the phase transition.

3: A solution of $MnCl_2{\cdot}4H_2O$ (0.495 g) in H_2O (25 mL, room temperature) was added to a solution of $K_3[Fe(CN)_6]$ (0.823 g) and RbCl (3.023 g) in H_2O (25 mL, 43 °C). The resulting solution was stirred at a constant speed of 5.5 rotations per second. The solution was added instantaneously (≈5 s for 25 mL). A brown powder precipitated and this was centrifuged and washed with room-temperature water (2×). The sample was dried overnight in vacuo. Yield (based on Mn): 727 mg (86%). $Rb_{0.61}Mn[Fe(CN)_6]_{0.86}{\cdot}2.71H_2O$ (338.07): calcd. C 18.34, H 1.61, Fe 14.21, Mn 16.20, N 21.39, Rb 15.49; found C 19.02, H 1.30, Fe 14.26, Mn 16.20, N 21.22, Rb 15.49.

Microanalyses: Analysis for C, H, and N were performed after combustion at 850 °C by using IR detection and gravimetry with a Perkin–Elmer 2400 series II device. Fe, Mn, Rb, and K concentration were determined by the Service Central d'Analyse du CNRS (Vernaison) by using ICP–AES (inductively coupled plasma atomic emission spectroscopy) after acid digestion in H_2SO_4/HNO_3. Standard deviations of the measured metal concentrations were typically around 2 rel.-%. The O and H atoms were assumed to be the only others elements present in the samples and the H_2O content was obtained by difference to 100%. (The K concentration was found negligible.).

Magnetic Studies: The magnetic properties were measured at various cooling and heating rates under a field of 0.1 T by using a Quantum Design MPMS superconducting quantum interference device magnetometer. The experimental data were corrected for the diamagnetic contribution using Pascal's constants.

Differential Scanning Calorimetry (DSC): DSC analysis was carried out with a Netsch DSC 204 instrument under helium purging gas (20 $cm^3\,min^{-1}$) at a heating/cooling rate of 10 K min^{-1}. Temperature and enthalpy were calibrated by using the melting transition of standard materials (Hg, In, Sn). The uncertainty in the transition enthalpy (ΔH_{HL}) and entropy (ΔS_{HL}) was estimated to ca. 10% owing to the subtraction of the unknown baseline.

Raman Spectroscopy: Raman spectra were collected between 300 and 80 K by using a LabRAM-HR (Jobin–Yvon) Raman microspectrometer and a Linkam THMS-600 cryostage. The 632.8 nm line of a HeNe laser was used as the excitation source and a spectral resolution of ca. 1 cm^{-1} was obtained. Least-square fitting of the Raman peaks was carried out with the assumption of Lorentzian line shapes.

X-ray Powder Diffraction: Measurements were carried out in Bragg–Brentano geometry by using a Bruker D8 Advance diffractometer operating with Cu-K_α radiation. The finely ground powder was attached to the sample holder with Vaseline. Data were collected between 2θ = 10° and 2θ = 70° with a step size of 0.02°, measuring for 4 s per step. The sample was rotated at 60 rpm. The resulting diffraction profiles were analyzed by using the GSAS software suite.[28]

Mössbauer Spectroscopy: ^{57}Fe Mössbauer spectra were recorded by using a conventional constant-acceleration type spectrometer equipped with a 50 mCi ^{57}Co source and a flow-type, liquid helium cryostat. Spectra of the powder samples (ca. 30 mg) were recorded between 5 and 300 K. Least-square fitting of the Mössbauer spectra was carried out with the assumption of Lorentzian line shape by using the Recoil software package.[29]

Supporting Information (see footnote on the first page of this article): Evolution of the Raman linewidths of the CN stretching modes, stoichiometry relationships, phase-transition temperature and stoichiometry relationships, and powder X-ray diffraction data.

Acknowledgments

L. Rechignat and J.-F. Meunier (LCC-CNRS) are acknowledged for experimental assistance. This work was financially supported by the COST D35 European program and the Zernike Institute for Advanced Materials.

[1] T. Mallah, S. Thiébaut, M. Verdaguer, P. Veillet, *Science* **1993**, *262*, 1554.
[2] M. Verdaguer, A. Bleuzen, V. Marvaud, J. Vaissermann, M. Seuleiman, C. Desplanches, A. Scuiller, C. Train, R. Garde, G. Gelly, C. Lomenech, I. Roseman, P. Veillet, C. Cartier, F. Villain, *Coord. Chem. Rev.* **1999**, *190–192*, 1023.
[3] O. Sato, T. Iyoda, A. Fujishima, K. Hashimoto, *Science* **1996**, *272*, 704.
[4] V. Escax, A. Bleuzen, C. Cartier, F. Villain, A. Goujon, F. Varret, M. Verdaguer, *J. Am. Chem. Soc.* **2001**, *123*, 12536.

[5] V. Escax, A. Bleuzen, J. P. Itié, P. Munsch, F. Varret, M. Verdaguer, *J. Phys. Chem. B* **2003**, *107*, 4763.
[6] S. Ohkoshi, K. Arai, Y. Sato, K. Hashimoto, *Nat. Mater.* **2004**, *3*, 857.
[7] N. Shimamoto, S. Ohkoshi, O. Sato, K. Hashimoto, *Inorg. Chem.* **2002**, *41*, 678.
[8] S. Ohkoshi, H. Tokoro, K. Hashimoto, *Coord. Chem. Rev.* **2005**, *249*, 1830.
[9] S. Ohkoshi, H. Tokoro, M. Utsunomiya, M. Mizuno, M. Abe, K. Hashimoto, *J. Phys. Chem. B* **2002**, *106*, 2423.
[10] Y. Moritomo, K. Kato, A. Kuriki, M. Takata, M. Sakata, H. Tokoro, S. Ohkoshi, K. Hashimoto, *J. Phys. Soc. Jpn.* **2002**, *71*, 2078.
[11] Y. Moritomo, K. Kato, A. Kuriki, M. Takata, M. Sakata, H. Tokoro, S. Ohkoshi, K. Hashimoto, *J. Phys. Soc. Jpn.* **2003**, *72*, 2698.
[12] Y. Moritomo, M. Hanawa, Y. Ohishi, K. Kato, M. Takata, A. Kuriki, *Phys. Rev. B* **2003**, *68*, 144106.
[13] S. Gawali-Salunke, F. Varret, I. Maurin, C. Enachescu, M. Malarova, K. Boukheddaden, E. Codjovi, H. Tokoro, S. Ohkoshi, K. Hashimoto, *J. Phys. Chem. B* **2005**, *109*, 8251–8256.
[14] S. Cobo, R. Fernandez, L. Salmon, G. Molnár, A. Bousseksou, *Eur. J. Inorg. Chem.* **2007**, 1548.
[15] S. Ohkoshi, T. Matsuda, H. Tokoro, K. Hashimoto, *Chem. Mater.* **2005**, *17*, 81.
[16] H. Tokoro, S. Ohkoshi, K. Hashimoto, *Appl. Phys. Lett.* **2003**, *82*, 1245.
[17] H. Tokoro, T. Matsuda, K. Hashimoto, S. Ohkoshi, *J. Appl. Phys.* **2005**, *97*, 10M508.
[18] H. Tokoro, S. Miyashita, K. Hashimoto, S. Ohkoshi, *Phys. Rev. B* **2006**, *73*, 172415.
[19] H. Tokoro, T. Matsuda, S. Miyashita, K. Hashimoto, S. Ohkoshi, *J. Phys. Soc. Jpn.* **2006**, *75*, 85004.
[20] H. Tokoro, T. Matsuda, T. Nuida, Y. Moritomo, K. Ohoyama, E. D. Loutete Dangui, K. Boukheddaden, S. Ohkoshi, *Chem. Mater.* **2008**, *20*, 423.
[21] E. J. M. Vertelman, E. Maccallini, D. Gournis, P. Rudolf, T. Bakas, J. Luzon, R. Broer, A. Pugzlys, T. T. A. Lummen, P. H. M. van Loosdrecht, P. J. van Koningsbruggen, *Chem. Mater.* **2006**, *18*, 1951.
[22] E. J. M. Vertelman, T. T. A. Lummen, A. Meetsma, M. W. Bouwkamp, G. Molnar, P. H. M. van Loosdrecht, P. J. van Koningsbruggen, *Chem. Mater.* **2008**, *20*, 1236–1238.
[23] T. Yokoyama, H. Tokoro, S. Ohkoshi, K. Hashimoto, K. Okamoto, T. Ohta, *Phys. Rev. B* **2002**, *66*, 184111.
[24] J. Luzon, M. Castro, E. J. M. Vertelman, R. Y. N. Gengler, P. J. van Koningsbruggen, O. Molodtsova, M. Knupfer, P. Rudolf, P. H. M. van Loosdrecht, R. Broer, *J. Phys. Chem. A* **2008**, *112*, 5742.
[25] S. Ohkoshi, S. Saito, T. Matsuda, T. Nuida, H. Tokoro, *J. Phys. Chem. C* **2008**, *112*, 13095.
[26] N. N. Greenwood, T. C. Gibb, *Mössbauer spectroscopy*, Chapman and Hall Ltd., London **1971**.
[27] K. Boukheddaden, F. Varret, *Hyperfine Interactions* **1992**, *72*, 349.
[28] A. C. Larson, R. B. Von Dreele, *General Structure Analysis System (GSAS)*, Los Alamos National Laboratory Report (LAUR), **2004**, pp. 86–748.
[29] http://www.isapps.ca/recoil/.

Received: October 6, 2008
Published Online: January 14, 2009

